form of neutral TTF, and K^+ is introduced into the film. The subsequent oxidation causes introduction of Br^- into the film and probably the nucleation of $TTFBr_{0.7}$ structure. After a few cycles, some of these grow into the large needle crystals which are not electroactive and remain in the conductive $TTFBr_{0.7}$ form. This material is a known one-dimensional conductor.[11] The smaller zones, perhaps representing organized TTF^+Br^- structures within the Nafion channels, remain electroactive and account for the CV waves and color changes seen on cycling. Apparently these do not grow into crystals because of the hydrophobic zones surrounding them that are depleted of TTF^+.

The needle crystals are conductive and contact the substrate,[15] since electrodeposition of Cu was found on these. The spacing between these as observed by microscopy (~ 10 μm) is generally consistent with the spacings found in electrochemical measurements with analysis of the data according to the models for partially covered electrodes. Moreover, the RDE $1/i_l$ vs. $\omega^{-1/2}$ plots for reduction of ferricyanide show intercepts that are independent of whether the NAF,TTF film is in the oxidized or reduced state. This suggests that the overall area of conductive sites and their distribution are independent of the state of oxidation of the polymer film and point to the needle crystals as the conductive surface sites. The conduction within the small electroactive zones must also be rather rapid, however. The film redox processes show "thin-layer" behavior even at rather slow scan rates, under conditions where other species incorporated into Nafion (e.g., $Ru(bpy)_3^{2+}$) show "diffusion-controlled" behavior. While this might be ascribed to the effect of the needle crystals that penetrate the film acting as internal wires, the distance between these and the electroactive zones is of the order or larger of the film thickness itself. Thus we feel that there is also enhanced charge transfer within the electroactive zones. The major contribution to charge transfer to solution species reacting at the polymer film surface (e.g., $Fe(CN)_6^{3-}$) is probably made by the conductive needle crystals, however.

We might also contrast the behavior of these polymer films and those previously studied in which TTF was incorporated by covalent attachment to the polymer backbone.[16] While evidence of formation of TTF_2^{2+} species in the latter polymer was obtained, no crystallization or long-range ordering was observed, probably because of lesser flexibility in the chains and the absence of the organized channel structure which exists in Nafion.

(15) The experiment shown in Figure 2b suggests that mediated charge transfer within the polymer layer between substrate and the crystals does not occur. Note that the net cathodic current on the far right ($E = -0.1$ V) is the same as that preceding the TTF^+ reduction peak. At these potentials only TTF in the neutral form is present, and mediated transport is unlikely.

(16) Kaufman, F. B.; Schroeder, A. H.; Engler, E. M.; Kramer, S. R.; Chambers, J. Q. *J. Am. Chem. Soc.* **1980**, *102*, 483.

Conclusions

The model of a biconductive polymer layer of Nafion with incorporated TTF species, in which both electronic and ionic conduction occurs, appears to be confirmed by these experiments. The electronic conduction to solution species takes place predominantly via μm-sized needle crystals of $TTFBr_{0.7}$. Separate electroactive TTF^+Br^- zones also exist in the film, however. Preliminary experiments suggest that these films might be useful as protective layers on semiconductor electrodes and perhaps might also be employed to incorporate catalysts onto electrode surfaces.

Acknowledgment. This research was supported by a grant from the National Science Foundation (CHE 7903729). The assistance of Dr. Michael Schmerling in obtaining the electron micrographs and of Cindy Williamson in obtaining the optical micrographs is gratefully acknowledged.

Registry No. NAF, 39464-59-0; TTF^+, 35079-56-2; Pt, 7440-06-4; Ta, 7440-25-7; SnO_2, 18282-10-5; Si, 7440-21-3; FeY^{2-}, 15651-72-6; TTF, 31366-25-3; KBr, 7758-02-3; ferricyanide, 13408-62-3; copper, 7440-50-8.

Photochemistry in Polymerized Microemulsion Systems[1]

S. S. Atik and J. K. Thomas*

Contribution from the Chemistry Department, University of Notre Dame, Notre Dame, Indiana 46556. *Received December 28, 1981*

Abstract: The preparation of polymerized microemulsions, P-μE, by polymerization of a microemulsion consisting of cetyltrimethylammonium bromide, hexanol, styrene, and divinylbenzene is reported. Typically the P-μE are well defined and show radii in the range 200 to 400 Å. Unlike micelles or microemulsions, the P-μE are quite stable to dilution, and remain intact over a wide range of concentrations. These properties are established by using photophysical properties of guest molecules in the systems. The P-μE exhibit two distinct sites of solubilization for a guest molecule: one in the surfactant coating and the second in the polymerized styrene core of the particle. The guest molecules are bound much more strongly to P-μE than to micelles. The two sites of guest solubilization in P-μE lead to unique effects on the quenching reactions involving excited guest and a quencher. For example, the excited guest molecules in the surfactant region are readily quenched by I^- or O_2, while those in the polymer are relatively unaffected. These systems provide vehicles for studying photoinduced reactions over controlled separation distances where the effects of diffusion are minimized.

Introduction

The past decade has seen considerable interest in the use of organized assemblies, i.e., micelles, microemulsions, vesicles, etc., to influence radiation-induced reactions.[2-5] A most useful extension of the work lies in the use of cross-linked polymerized assemblies,[6,7] in particular as applied to vesicular systems. Polymerization lends stability and permanence to these kinetic structures and secures solubilized moelcules more tightly.

(1) We wish to thank the NSF for support of this work (Grant CHE 24867).
(2) J. Fendler, *Acc. Chem. Res.*, **9**, 1953 (1976).
(3) N. Turro, M. Grätzel, and A. Braun, *Angew. Chem.*, **19**, 675 (1980).
(4) J. K. Thomas, *Chem. Rev.*, **80**, 283 (1980).
(5) T. S. Chen and J. K. Thomas, *J. Chem. Educ.*, **58**, 140 (1981).
(6) See *Chem. Eng. News.*, **59** (Aug 3), 8 (1981).
(7) L. Gras, H. Ringsdorf, and H. Schupp, *Angew. Chem., Int. Ed. Engl.*, **20**, 305 (1981).

0002-7863/82/1504-5868$01.25/0

We recently reported details of the preparation and characterization of an oil in water (O/W) polymerized microemulsion (P-μE) system composed of styrene–divinylbenzene as the oil droplet, stabilized by the surfactant cetyltrimethylammonium bromide (CTAB) and cosurfactant hexanol.[8] The size and distribution of the P-μE particles were investigated by electron microscopy which provided a visual view of these otherwise (unpolymerized) elusive and labile μE particles.

We now wish to report a more detailed account of the stability of these P-μE particles, and their unique mode of interactions with polar, nonpolar, and ionic species as studied by photochemical techniques. The location and mobility of the solubilized molecules are investigated by steady-state and time-resolved fluorescence measurements.

The influence of the polymerized particles on photochemical processes is best demonstrated by comparison to the results obtained in micellar and unpolymerized (O/W) μE systems under similar conditions. A special and useful feature of the polymerized colloidal particles is that they combine the structural properties of polymer films with the simplicity and convenience of studying photochemistry in solution.

Experimental Section

Preparation and Polymerization of (O/W) Cetyltrimethylammonium Bromide Microemulsion (CTAB-μE). An oil in water μE composed of 1.0 g of cetyltrimethylammonium bromide (CTAB), 0.5 g of hexanol, and 1.0 g of 50% styrene–divinylbenzene in 50 mL of water was carefully prepared by slowly adding the water to a stirred mixture of the other components to yield a slightly bluish clear solution. A 0.1% solution (w/w) of initiater AIBN (based on monomer) is then solubilized in the system followed by removal of O_2 (by gentle N_2 bubbling for 5 min), and finally the system is heated in an oil bath (50 °C) until complete polymerization is achieved as determined spectrophotometrically. Proper dilution with water is then made to give a 0.01 M CTAB–P-μE solution (P-μE indicates polymerized microemulsion), which was used in most of the experiments described in the present report.

The size of the P-μE particles was determined by two techniques: (a) electron microscope and (b) Nicomp particle analyzer. Results obtained by the two methods are found to be in good agreement.

The specimen for the electron microscope was made by drying one drop of 1.0×10^{-4} M CTAB–P-μE on a copper grid which was previously coated with a thin film of carbon deposited by vacuum evaporation. This was then followed by adding another drop of phosphotungstic buffer (pH 7) and then dried with a filter paper.

The electron microscope used was H-600, and the magnifications were generally 100 000. The size of the spherically shaped P-μE particles was directly measured from the electron photomicrograph to yield a particle diameter of 310 ± 20 Å.

Nicomp Particle Analyzer. This light- (single-mode 6328 A He–Ne laser) scattering computerized instrument utilizes the theory of Rayleigh scattering of translational Brownian particles to compute the mean translational diffusion constant $\bar{D}$. This is then used to determine the average hydrodynamic radius $\bar{R}$ using the Stokes–Einstein relationship for spherical particles, $D = kT/6\pi\eta R$.

A built-in microcomputer system performs rapid quadratic least-squares fit to the data, yielding $\bar{D}$, $\bar{R}$, σ (normalized standard deviation of the intensity-weighted distribution of diffusion constants), and χ-squares goodness of fit. A typical result obtained for 1.0×10^{-3} M CTAB–P-μE is: $\bar{D} = 1.20 \times 10^{-7}$ cm^2/s, $\bar{R} = 177$ Å, $\sigma = 0.50$, $\chi = 2.20$.

Materials. Styrene (Eastman) and divinylbenzene (Polyscience) were purified prior to use by removal of inhibitor by multiple washes with 5% sodium hydroxide solution followed by multiple-distilled water washes and finally vacuum distillation. Cetyltrimethylammonium bromide (CTAB) obtained from Sigma was twice recrystallized from absolute ethanol–acetone; cetylpyridinium chloride (CPC) (Eastman), pyrene (Aldrich), pyrenebutyric acid (PBA) (Pfaltz and Bauer), and pyrenedodecanoic acid (PDA) were used.

Experimental Results and Discussion

Stability to Dilution. A point of interest is the stability of the polymerized microemulsion (P-μE) with respect to dilution. It is important to determine whether the polymerized core of the P-μE comes out of solution below the critical micelle concentration, cmc, of the emulsifying surfactant.

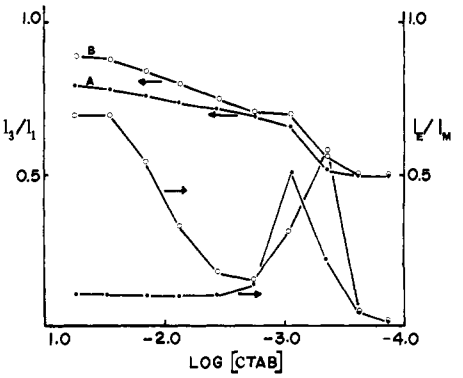

Figure 1. Observed changes in I_3/I_1 and I_e/I_m upon dilution of CTAB micellar solution (A) and CTAB–toluene-μE system (see text).

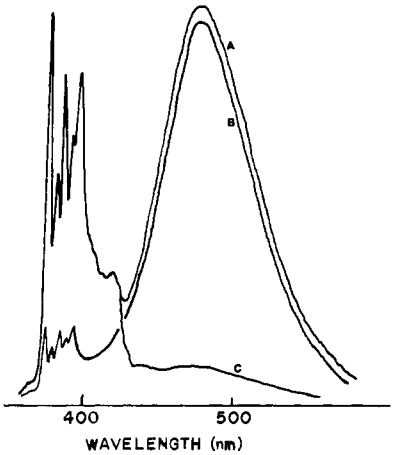

Figure 2. Total fluorescence spectra for 5.0×10^{-4} M P in (A) 0.01 M CTAB, (B) 0.01 M CTAB–toluene-μE, (C) 0.01 M CTAB–P-μE

The method used for this study is the fine structure of pyrene, P, fluorescence (namely I_3/I_1), which is now well recognized as being sensitive to the polarity of the probe's microenvironment.[9] In order to check the validity of the technique in detecting microscopic phase changes, it was first used for a CTAB micelle and a CTAB-μE (O/W) consisting of 1.0 g of CTAB, 0.5 g of hexanol, and 1.0 g of toluene in 50 mL of water. Both solutions initially contained 2.0×10^{-4} M P. Figure 1 shows the simultaneous variations in I_3/I_1 and I_e/I_m where I_e and I_m are the excimer and monomer fluorescence intensities monitored at 470 and 394 nm, respectively. It is evident that in each case, both I_3/I_1 and I_e/I_m values undergo an abrupt change near the cmc of the surfactant (9.4×10^{-4} M), suggesting that such a μE is not stable at [surfactant] < cmc. Above the cmc the I_3/I_1 value is suggestive of a hydrophobic microenvironment for P, while below the cmc the observed value is similar to that obtained in water which would indicate that below the cmc the μE system disintegrates into its monomeric components which dissolve molecularly in water. On the other hand, in the case of a P-μE of the same composition as above (using 50% styrene–divinylbenzene instead of toluene), the observed value for I_3/I_1 remained essentially unchanged upon dilution (being 0.91 and 0.88 for 0.05 M CTAB–P-μE and 1.0×10^{-5} M CTAB–P-μE, respectively). It is therefore concluded that the P-μE particle remains intact and remarkably stable even at a surfactant concentration which is two orders of magnitude below the cmc. Moreover, it is important to note here that in sharp contrast to CTAB–toluene-μE, pyrene excimer formation is greatly reduced, and this is indicative of a very rigid microenvironment for P. Therefore it seems reasonable to suggest that the most likely site for P is the polymerized core of the P-μE where molecular diffusion would be very much restricted.

(8) S. S. Atik and J. K. Thomas, *J. Am. Chem. Soc.*, **103**, 4367 (1981).

(9) M. Kalyanasundaram and J. K. Thomas, *J. Am. Chem. Soc.*, **99**, 2039 (1977).

Table I. Comparison of Excimer Formation Data, I_e/I_m

	system[a]		
	A	B	C
5.0×10^{-4} M P	1.35	5.10	0.12
1.0×10^{-3} M P	3.24		0.25
5.0×10^{-4} M PBA	0.50	0.30	0.40

[a] A, 0.01 M CTAB; B, 0.01 M CTAB–toluene-μE; C, 0.01 M CTAB-P-μE.

Table II. Oxygen Fluorescence Quenching Data for P (5.0×10^{-6} M) and PBA (5.0×10^{-6} M) Bound to Micelles, O/W μE and P-μE

		P		PBA	
		τ, ns	Q[a]	τ, ns	Q
0.01 M CTAB	N_2	170	0.0	130	0.0
	air	116	0.32	100	0.23
	O_2	53	0.70	53	0.63
0.01 M CTAB–toluene-μE (O/W)	N_2	240	0.0	168	0.0
	air	87	0.69	90	0.48
	O_2	33	0.88	41	0.76
0.01 M CTAB–P-μE	N_2	260 (425)[b]	0.0	135	0.0
	air	180 (425)	0.14	97	0.22
	O_2	150 (320)	0.32	75	0.43

[a] Q is a quenching factor defined by $(I_0 - I)/I$, where I_0 and I are fluorescence intensities measured at 394 nm in the absence (N_2) and presence of O_2 (air). [b] Initial and final lifetimes calculated from the observed nonexponential decays.

Figure 2 compares the emission spectra obtained for 5.0×10^{-4} M P in 0.01 M CTAB, 0.01 M CTAB–toluene-μE, and 0.01 M CTAB–P-μE. It is seen that I_e/I_m increases drastically in going from micelle to toluene-μE, which is attributed to the much smaller microviscosity of the μE, where P would be located preferentially in the toluene oil drop of the μE particle. On the other hand, excimer emission is noted to be extremely weak in P-μE, suggesting that a very high microviscosity is sensed by P.

Table I shows the measured values of (I_e/I_m) for P and PBA in the varied systems. In sharp contrast to P, only small variations in (I_e/I_m) are observed for PBA in the three aggregate assemblies, and this is probably suggestive of a similar solubilization site near the Stern layer.

Relative Binding Strength of P-μE and Micelles to Hydrophobic Probes (Pyrene). Previous work showed that the solubilization site of P is close to the head group region of CTAB micelle.[10] However, in the polymerized μE the results presented above suggest that P is not located near the Stern layer but is rather predominantly embedded in the polymer matrix of the P-μE particle. If such an interpretation is correct, then one predicts that the hydrophobic binding of P to the P-μE would be much stronger than to micelles.

To investigate the relative binding strength of the two systems, cetylpyridinium chloride, CPC, was chosen as a suitable representative micelle. The CPC monomer is found to be a very efficient quencher of P* fluorescence ($k_q = 1.5 \times 10^{10}$ M^{-1} s^{-1}) in acetonitrile, so that P* bound to CPC micelle is statically quenched, while P* solubilized in the P-μE is protected. The quenching mechanism is found to involved an electron transfer from P* to CPC. Figure 3 shows the transient absorption spectrum of the pyrene cation radical obtained immediately following and 200 μs after the 6-ns laser pulse, 3370-Å light. The pyrene cation radical concentration monitored at 450 nm was found to decay by mixed first- and second-order processes over a period of several hundred microseconds. The surprising long lifetime of P^+ can perhaps be explained by a very fast electron exchange between reduced CPC and surrounding CPC molecules in the micelle, thus inhibiting the back-electron-transfer reaction. In a solution

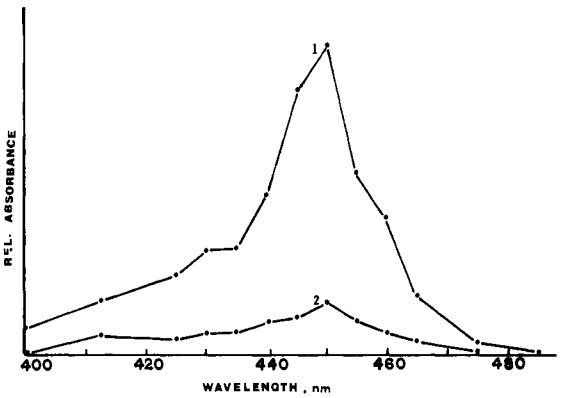

Figure 3. Transient absorption spectra observed immediately (1) and 200 μs (2) after the 6-ns laser pulse for air-equilibrated solution of 5.0×10^{-5} M P in 0.05 M CPC.

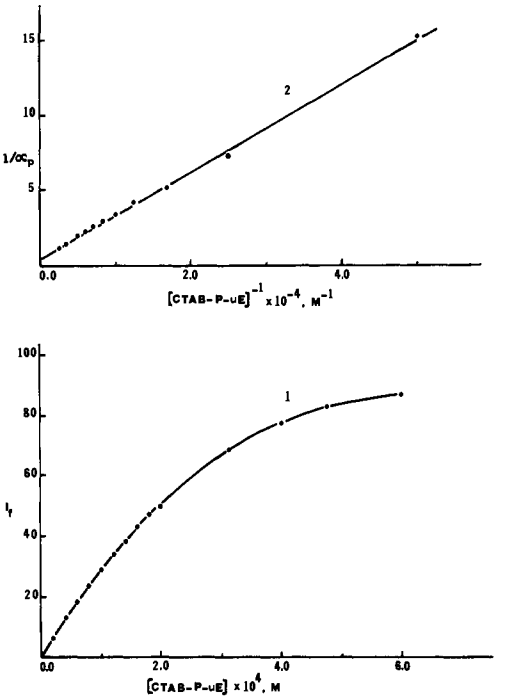

Figure 4. (1) Change in the intensity of the fluorescence (394 nm) of 5.0×10^{-6} M P in 0.01 M CPC upon titration with CTAB–P-μE. (2) A double reciprocal plot of α_p^{-1} against $[CTAB\text{–}P\text{-}\mu E]^{-1}$.

containing P-μE particles and CPC micelles, the observed fluorescence is a measure of P partitioning in favor of the P-μE. Therefore, the extent of binding of P to the P-μE can be easily monitored by fluorescence intensity measurements. Figure 4 shows the recovery of P* fluorescence (monitored at 394 nm) in a solution containing 5.0×10^{-6} M P in 0.01 M CPC (where P* fluorescence is 100% quenched) with added CTAB–P-μE. This recovery is attributed to the transfer of P from the CPC micelle where it is statically and completely quenched to the P-μE particle. This transfer process can be described by

$$M\cdot P \rightleftharpoons M + P \qquad 1/K_m \tag{1a}$$

$$P + P\text{-}\mu E \rightleftharpoons P\text{-}\mu E\cdot P \qquad K_p \tag{1b}$$

where M·P and P-μE·P are micelle bound pyrene and polymerized μE bound pyrene, respectively, M is free CPC micelle in solution, and K_m and K_p are the binding constants of P to M and P-μE, respectively. Equation 1a describes the dissociation of P from the micelle and eq 1b expresses its capture by the P-μE particle. Using these two equations, it can be shown that

$$K = \frac{K_p}{K_m} = \frac{[P\text{-}\mu E\cdot P][M]}{[M\cdot P][P\text{-}\mu E]} \tag{2}$$

(10) M. Almgren, F. Greiser, and J. K. Thomas, *J. Am. Chem. Soc.*, **101**, 279 (1979).

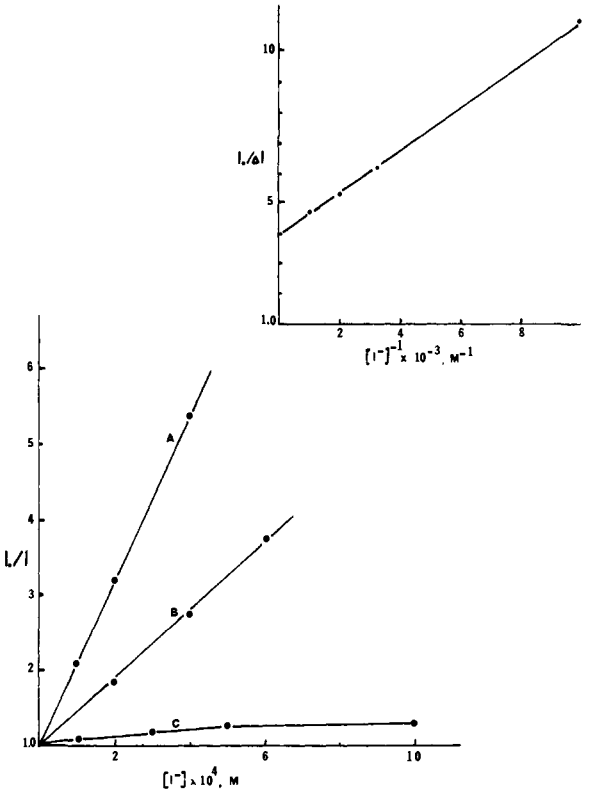

Figure 5. Stern–Volmer fluorescence quenching plots for N_2-bubbled solution of 5.0×10^{-6} M P in (A) 0.01 M CTAB, (B) 0.01 M CTAB–toluene-μE, (C) 0.01 M CTAB-P-μE. Insert: A modified Stern–Volmer plot for the experimental data used to produce curve C.

where K reflects the resulting transfer process of P from M to P-μE:

$$\text{P-}\mu\text{E} + \text{M}\cdot\text{P} \rightleftharpoons \text{P-}\mu\text{E}\cdot\text{P} + \text{M} \tag{3}$$

Using eq 2, the following relationship can be readily obtained,

$$\frac{1}{\alpha_p} = 1 - \frac{[\text{M}]}{K[\text{P-}\mu\text{E}]} = 1 + \frac{[\text{M}]N_p}{K[\text{CTAB–P-}\mu\text{E}]} \tag{4}$$

where α_p is the fraction of P bound to P-μE which is given by $\Delta I_F/\Delta I^0_F$ where ΔI_F ($= I_{obsd} - I_M$) is the observed change in the fluorescence intensity I_F upon addition of CTAB-P-μE; I_M is the fluorescence intensity in the CPC micellar system in the absence of CTAB-P-μE, which assumes a value of 0, and $\Delta I_F{}^\circ$ ($=I_{max} - I_M$) is the maximum observed ΔI_F at (CTAB-P-μE) $\rightarrow \infty$ obtained from a plot of $(\Delta I_F)^{-1}$ vs. $[\text{CTAB-P-}\mu\text{E}]^{-1}$.

A plot of α_p^{-1} vs. $[\text{CTAB-P-}\mu\text{E}]^{-1}$ (Figure 4) is indeed found to be linear in accordance with eq 3 with a slope of 2.8×10^{-4} M. Taking the literature cmc of 1.0×10^{-3} M and an aggregation number of 100 for the CPC micelle, and using the estimated 2×10^4 aggregation number for the CTAB-P-μE,[11] K is calculated to be 6.8×10^3.

Accessibility to Surface-Absorbed Quenchers of P Bound to P-μE Particles. Quenching of the fluorescence of 5.0×10^{-6} M P solubilized in 0.01 M CTAB-P-μE was carried out using I^-: this quencher is restricted to the Stern-layer region of the P-μE particle. A surfactant quencher, CPC, was also used, which binds to the P-μE particle with the pyridinium quenching residue located in the head group region of the CTAB surfactant layer which coats the polymerized latex sphere. Figures 5 and 6 show that the quenching data exhibited unconventional Stern–Volmer plots with both quenchers.

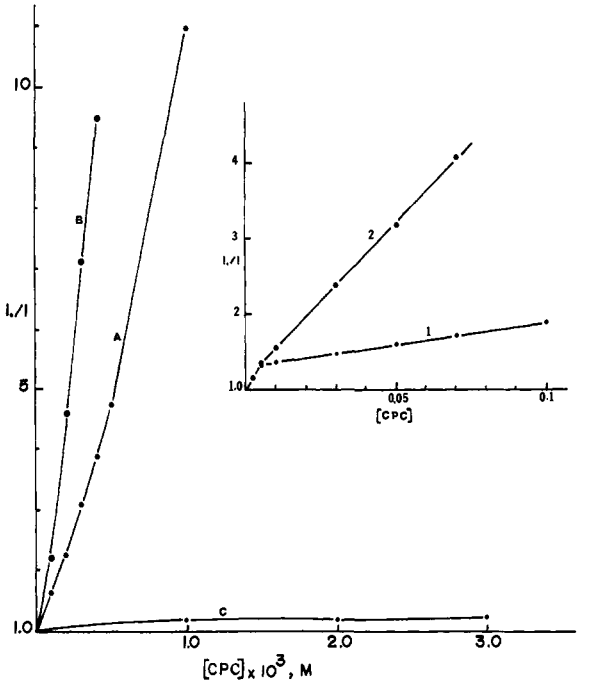

Figure 6. Stern–Volmer fluorescence quenching type plots for N_2-bubbled solutions of 5.0×10^{-6} M P in (A) 0.01 M CTAB, (B) 0.01 M CTAB–toluene-μE, (C,1) 0.01 M CTAB-P-μE, (2) 0.001 M CTAB-P-μE.

The fluorescence decay of solubilized P in the absence of quencher is noted to be nonexponential but adequately described by a double exponential function of the form

$$I_F(t) = I_F(0)\left(\alpha_m e^{-t/\tau_m{}^0} + \alpha_p e^{-t/\tau_m{}^0}\right) \tag{5}$$

where α_m and α_p are the two fractions of P* having lifetimes $\tau_m{}^0$ and $\tau_p{}^0$, respectively, and $\alpha_m + \alpha_p = 1.0$. Under undegassed conditions, an optimal fit to P* fluorescence decay is achieved with $\alpha_m = 0.25$, $\tau_m{}^0 = 180$ ns, and $\tau_p{}^0 = 425$ ns.

Quenching of P* Fluorescence with I^-. Added I^- appeared only to enhance the decay of the initial component of P* decay, leaving the lifetime of the second component unaffected. Such a fluorescence decay dependence on (I^-) is consistent with eq 4 and can therefore be represented by

$$I_F(t) = I_F(t=0)\left\{\alpha_m e^{-[(\tau_m{}^0)^{-1} + k_q[I^-]]t} + \alpha_p e^{-t/\tau_p{}^0}\right\} \tag{6}$$

Thus when the decay time t is large and $(\tau_p{}^0)^{-1} \gg \{(\tau_m{}^0)^{-1} + k_q[I^-]\}$, only the second term of eq 6 survives, i.e.,

$$I_F(t) = I_F(t=0)\alpha_p e^{-t/\tau_p} \tag{7}$$

or

$$\ln [I_F(t)/I_F(t=0)] = \ln \alpha_p - t/\tau_p{}^0 \tag{8}$$

From the long-lived portion of the decay curves, $\ln[I_F(t)/I_F(t=0)]$ vs. t, extrapolating to $t = 0$, one obtains $\ln \alpha_p$ as the intercept. A value of $\alpha_p = 0.25 \pm 0.5$ is determined from this transient fluorescence quenching experiment which is in good agreement with results obtained in the absence of I^-. In the limit of added I^-, where $1/\tau_p{}^0 >> (\tau_m{}^{-1} + k_q[I^-])$ for all values of t, the initial fast part of the decay disappears completely to give rise to an exponential decay with a lifetime of $\tau_p{}^0 = 425$ ns. This result suggests that P experiences two isolated sites of solubilization, one accessible to ionic surface quenchers constituting 22% of total (P) and therefore probably located in the micellar surfactant layer of P-μE. The remaining 80% of unquenchable P* is likely to be immobilized in the polymer matrix which would impose a great restriction on its diffusion to the surface within its lifetime.

(11) Using 2 mL as a reasonable estimate of the total volume of the P-μE particles described in the Experimental Section and the experimentally determined particle radius (177 Å), the surfactant aggregation number of a P-μE particle is determined to be $\sim 2 \times 10^4$. Consequently, the calculated surface area per surfactant head group is found to be 21 Å^2 which is a reasonable estimate used on monolayer (E. D. Goddard, "Monolayers", *Adv. Chem. Ser.*, No. 144 (1975)) and micelle packing studies (C. Tanford, "The Hydrophobic Effect: Formation of Micelles and Biological Membranes", Wiley, New York, 1973).

In accordance with the results of the transient measurements, steady-state fluorescence intensity quenching (Figure 5) shows an initial fast quenching followed by no further quenching after about 25% of the total original fluorescence is quenched. A steady-state expression that describes this quenching pattern can be obtained by integration of eq 6 between the limits of $t = 0$ and $t = \infty$ to give

$$\frac{I_F}{I_F^0} = \frac{\alpha_m}{1 + k_{q_m}\tau_m^0[I^-]} + (1 - \alpha_m) \quad (9)$$

where I_F^0 and I_F are fluorescence yields in the absence and presence of I^-, respectively, τ_m^0 is the lifetime of P* in the micellar region of the P-μE in the absence of I^-, and k_{qm} is the bimolecular quenching rate constant for P* located in the micellar region. Rearranging (9) provides the following useful relationship

$$\frac{I_F^0}{I_F^0 - I_F} = \frac{1}{\alpha_m} + \frac{1}{\alpha_m k_{q_m}\tau_m^0[I^-]} \quad (10)$$

As predicted by eq 10, a linear plot of $I_F^0/(I_F^0 - I_F)$ vs. $[I^-]^{-1}$ is indeed realized (Figure 5, insert) yielding $\alpha_m = 0.25$ from the intercept and $k_{q_m} = 1.4 \times 10^{10}$ M^{-1} s^{-1} from the slope. Figure 5 also shows results of the quenching of P solubilized in the 0.01 M CTAB–toluene-μE (O/W) by I^- for comparison purposes. In this system the time-averaged homogeneous population of P* within the μE is reflected in the linearity of the Stern–Volmer plot as well as the first-order decay of P* in the absence ($\tau_F^0 =$ 240 ns) and presence of I^-. A good agreement is obtained between the steady-state and transient experiments yielding a bimolecular quenching rate constant $k_q = 1.8 \times 10^{10}$ M^{-1} s^{-1}.

Quenching of P* Fluorescence with CPC. Fluorescence quenching experiments were also conducted with the surfactant quencher, CPC, which would be strongly bound to the μE particle. In 0.01 M CTAB–toluene-μE system, the steady-state Stern–Volmer plot (Figure 6) exhibited an upward curvature resulting from the expected statistical distribution of the quenchers among the μE particles. The fluorescence decay in the presence of Q also was found to be nonexponential as anticipated from previous investigations.[12] On the other hand, different results are obtained in the case of a 0.01 M CTAB–P-μE system. Two distinct regions of quenching are observed as shown in Figure 6 (insert). The initial fast quenching is completed when ca. 25% of the total fluorescence is quenched and this is followed by a slower linear quenching with increasing (CPC). The fluorescence decay in the first region exhibits a fast component that decays faster with increasing CPC and a slow component that remains unaffected. At [CPC] = 0.01 M, only one exponential decay is observed ($\tau_F^0 =$ 425 ns) which remains invarient with increasing (CPC), and therefore suggests static quenching in this region.[13]

As in the case of I^- quenching, CPC appears to dynamically quench P* located in the micellar surfactant layer of the P-μE particle but is unable to quench P* intercalated into the polymer latex. The static quenching observed in the second region can be explained by the partitioning of P between free CPC micelles and P-μE particles (eq 1). This unusual fluorescence quenching pattern can be described by[12]

$$\frac{I_F}{I_F^0} = \alpha_m \sum_{n=0}^{\infty}\left(\frac{P_n}{1 + k_{q_m}\tau_m^{0n}}\right) + \frac{(1 - \alpha_m)N}{1 + K'[CPC]} \quad (11)$$

The first term in eq 8 represents a quenching quotient associated with quenching the fraction of P* located in the outer micellar layer of the P-μE particle by bound CPC quenchers. Assuming a Poisson distribution of quenchers where $P_n = \bar{n}^n e^{-\bar{n}}/n!$, $\bar{n} =$ (CPC)/(P-μE) and k_q is the first-order intramicellar quenching constant. The second term describes the static quenching effected by the transfer of P from the P-μE to the CPC micelle, where K' is a constant associated with this partitioning process, which is a function of (P-μE), and N is the aggregation number of CPC micelle. Because of the small contribution of the first term to the total fluorescence quenching, only quenching associated with the second term will be analyzed.

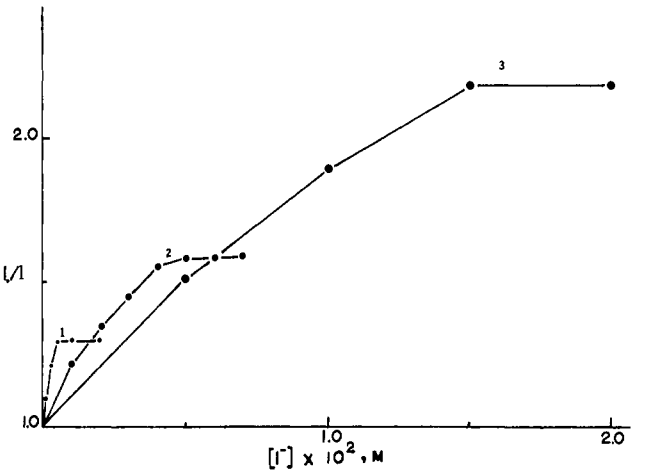

Figure 7. Fluorescence quenching curves for 5.0×10^{-6} M P in 0.01 M CTAB–P-μE: (1) without added CTAB and in the presence of (2) 0.05 M CTAB, (3) 0.1 M CTAB.

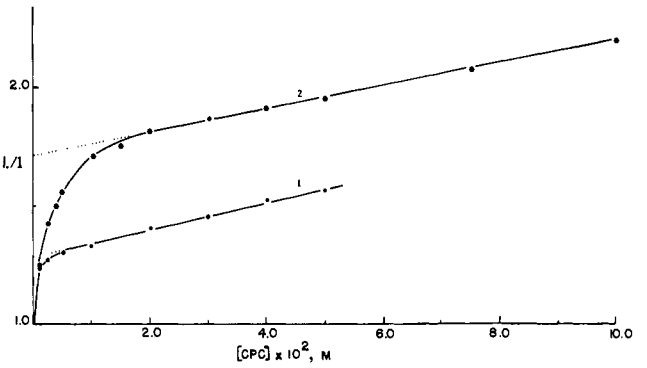

Figure 8. Quenching of the fluorescence of 5.0×10^{-6} M P in 0.01 M CTAB–P-μE by CPC in the absence (1) and presence (2) of 0.1 M CTAB.

According to eq 8, the slope of the linear quenching in the second region in Figure 6 is given by $K'/(1 - \alpha_m)N$. Using $\alpha_m = 0.25$ and $N = 100$, K' is calculated to be 450 and 1000 M^{-1} at 0.01 and 0.001 M CTAB–P-mE, respectively.

Effect of Added CTAB Micelles. Figure 7 shows the results of fluorescence quenching experiments carried out at 0.01 M CTAB–P-μE in the presence of added CTAB micelles. The figure includes quenching data obtained in the absence of added CTAB for the purpose of comparison. It is evident that the effect of added micelles on the quenching of the fluorescence of P* by I^- is twofold. First the rate of quenching is decreased because of the distribution of quenchers among the micelles, and second the maximum fluorescence quenching achieved is increased. In the absence of added CTAB, I^- could only quench 20% of P*; this value increases to 34% in the presence of 0.05 M CTAB and at 0.1 M CTAB it increases further to 55%. The increase in the fraction of P* accessible to I^- quenching with added CTAB can be understood in terms of the partitioning of P between the P-μE particles and free CTAB micelles as already discussed above. The fraction of micelle solubilized P would be expected to increase with (CTAB) according to eq 1.

Figure 8 also compares fluorescence quenching results obtained with and without added CTAB using CPC as a quencher of P*. There are two features to be noted here: first, the increase in the extent of dynamic quenching as is evident from the point of

(12) (a) S. S. Atik and L. A. Singer, *Chem. Phys. Lett.*, **59**, 519 (1978); (b) *ibid.*, **66**, 234 (1979); (c) S. S. Atik and J. K. Thomas *J. Am. Chem. Soc.*, **103**, 3550 (1981).

(13) S. S. Atik, C. L. Kwan, and L. A. Singer, *J. Am. Chem. Soc.*, **101**, 5696 (1979).

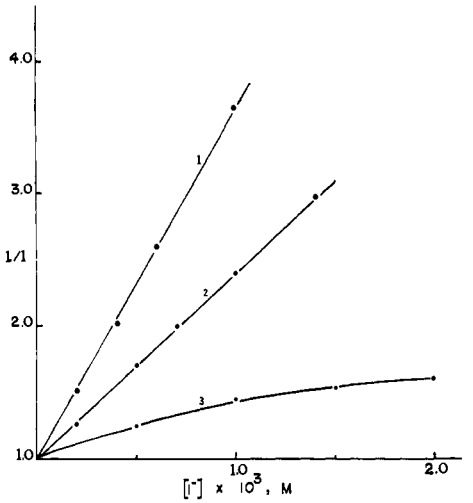

Figure 9. Fluorescence quenching data for 1.0×10^{-5} M of (1) PBA (PDA) in 0.01 M CTAB, (2) PBA in 0.01 M CTAB–P-μE, and (3) PDA in 0.01 M CTAB–P-μE.

intersection of the two distinct regions of quenching, and, second, the unchanging linear slope at high (CPC). As discussed above, the linear quenching observed at high (CPC) is attributed to static quenching resulting from the transfer of P from the P-μE particles to CPC micelles and therefore should be independent of added CTAB. On the other hand, the increase in the value of I_0/I that corresponds to the intersection point of the two regions is attributed to the increased fraction of quenchable P* incorporated into the added CTAB micelles.

Interactions of Pyrene Derivatives PBA and PDA with P-μE. Figure 9 compares the results of fluorescence quenching experiments for PBA and PDA in micelles and P-μE systems under similar conditions. Quenching of the fluorescence of PBA and PDA incorporated into CTAB micelle with I^- was found to be dynamic and identical for the two fluorescent probes ($k_q = 2.6 \times 10^{10}$ M^{-1} s^{-1}). This result indicates that the pyrenyl fluorophores of the two probes are equally accessible to quenchers present at the micellar surface but in dynamic equilibrium with those present in the aqueous bulk phase. It is therefore concluded that the pyrene chromophore of PDA is not strongly held to the hydrophobic micellar core where it might be protected from surface quenchers, but that it is dynamically solubilized in the micelle with the pyrene chromophore free to move within the entire micellar structure.

PBA and PDA interactions with the P-μE particle, however, are found to be markedly different. The fluorescence from PBA incorporated into the P-μE displayed a single exponential decay with a lifetime of 100 ns which is very similar to that observed in the CTAB micelle. On the other hand, the decay of PDA* in this system is distinctly nonexponential but adequately described by a sum of two exponentials (see eq 5). Best-fit to the experimental decay is achieved with $\alpha_m = 0.65$, $\tau_m^0 = 104$ ns, and $\tau_p^0 = 210$ ns. The homogeneity of the PBA* emitting population is confirmed by the linear Stern–Volmer quenching with I^- from which a bimolecular quenching rate constant $k_q = 1.4 \times 10^{10}$ M^{-1} s^{-1} is calculated. On the other hand, the heterogeneity of the sites occupied by PDA in the P-μE is also substantiated by the leveling-off effect observed for its fluorescence quenching by I^- (Figure 9). Analysis of the fluorescence quenching data according to eq 7 gave $\alpha_m = 0.70$ and $k_{q_m} = 6.0 \times 10^9$ M^{-1} s^{-1}. Moreover, added I^- seemed to continually decrease only the initial fast component of PDA fluorescence decay, leaving the second long component unchanged at $\tau = 230$ ns. These steady-state and transient fluorescence quenching experiments reveal that while PBA has a time-averaged dynamic solubilization site, PDA appears to have two isolated sites, one located in the outer surfactant layer of P-μE constituting about 70% and the remaining 30% is suggested to be embedded in the polymerized particle whereby its diffusion to the surface is greatly inhibited.

Oxygen Accessibility to the Two Distinct Regions of P-μE. Oxygen quenching of the fluorescence of aromatic hydrocarbons is commonly a diffusion-controlled process whose rate is a simple function of the viscosity of the medium and the concentration of O_2. However, in heterogeneous solutions of micelles, vesicles, proteins, and other biomacromolecules[14-16] O_2 quenching efficiency is a complex function of the effective (O_2) in the phase or aggregate containing the fluorescence probe, the microviscosity, and the accessibility of the probe to (O_2) in the bulk aqueous phase.

In the present study, the accessibility or the ease of O_2 penetration into the polymerized core and surfactant outer layer of the P-μE was investigated with steady-state fluorescence and lifetime measurements. Pyrene and PBA were chosen for probing the polymerized center and the micellar region, respectively. Fluorescence studies were also carried out in micellar and (O/W)-μE solutions under similar conditions for the purpose of comparison. Table I displays the results of steady-state fluorescence intensity quenching and fluorescence lifetime measurements for the three above-mentioned systems under N_2-bubbled, aerated, and oxygenated conditions. It is evident that P is most efficiently quenched by oxygen in the CTAB–toluene-μE system where P is expected to spend most of its time in the oxygen-rich oil droplet. However, in the P-μE system, O_2 quenching of P fluorescence is quite inefficient since it is predominantly located in the polymerized core where O_2 diffusion is greatly restricted. On the other hand, PBA* is more effectively quenched in the CTAB–toluene-μE than in either CTAB micelle or P-μE systems. It is noteworthy that the efficiency of quenching PBA* in P-μE is lower than in the CTAB micelle and much lower still than in CTAB–toluene-μE, which may be explained by the more restricted O_2 mobility in P-μE. In most cases there is a good agreement between the steady-state quenching data and measured fluorescence lifetimes, indicating a predominantly dynamic quenching.

Conclusion

The literature on the theory of emulsion polymerization is extensive. The basic theory is due to Harkins, and the experimental verification of the theory is reported by Smith and Ewart.[17,18] Emulsions are generally white opaque dispersions of a hydrocarbon liquid in an aqueous surfactant solution. A typical emulsion polymerization system would consist of 2–5 g of emulsifying surfactant (usually a fatty acid), 100 g of styrene, 0.1–0.5 g of potassium persulfate initiator, and 180 g of water. The polymerization is effected thermally (60 °C) to produce polystyrene latex spheres of ~ 1 μm in diameter.

On the other hand, (O/W) μE's are clear solutions composed of surfactant, cosurfactant (short-chain alcohol), and oil (hydrocarbon liquid) in water. The μE particles produced in this case, before polymerization consist of an oil droplet (<0.1 μm in diameter) surrounded by a layer of surfactant and cosurfactant molecules. After polymerization the solution remains clear but becomes slightly more bluish. The size of the spherical particles afforded in this system ranges from 200 to 400 Å in diameter.

From the point of view of a photochemist, or kineticist, the polymerized microemulsion particles possess many of the properties of the unpolymerized particles; i.e., the particles are charged and solubilize hydrophobic molecules. However, the polymerized system passes two distinct sites of guest solubilization and are stable to dilution over a large range of concentration. The two sites of solubilization are the surfactant mantle of the particle and the polymerized core. The former site shows photochemical and kinetic properties characteristic of micelles, i.e., diffusion of

(14) N. J. Turro, M. Aikawa, and A. Yekta, *Chem. Phys. Lett.*, **64**, 473 (1979).
(15) M. Almgren, F. Grieser, and J. K. Thomas, *J. Am. Chem. Soc.*, **102**, 3188 (1980).
(16) M. W. Vaughan and G. Weber, *Biochemistry*, **9**, 464 (1970).
(17) F. A. Bovey, I. M. Kolthoff, A. I. Medalia, and E. J. Meehan, "Emulsion Polymerization", Interscience, New York, 1955.
(18) P. J. Flory "Principles of Polymer Chemistry", Cornell University Press, New York, 1953.

reactants, etc. The core, however, is distinctly rigid and inhibits diffusion so that selection and energy transfer over distances of 10 Å are readily observed, as diffusion processes are inhibited. This behavior is useful in promoting long-range chemical processes of interest, and may also be used to enmesh or capture one of the reactants, on a long-term basis. The permanent nature of the polymerized particles enables the construction of a system containing two simple but distinct colloidal species, namely, the particle and a micelle. This provides the opportunity for promoting different photochemical reactions each with particle, followed by a pooling of the products in the aqueous bulk. Further studies to this end are now in progress.

Registry No. CTAB, 57-09-0; CPC, 123-03-5; PBA, 25338-56-1; PDA, 73451-05-5; I^-, 20461-54-5; styrene–divinylbenzene, 9003-70-7; pyrene, 129-00-0; oxygen, 7782-44-7.

Picosecond Laser Studies of Intramolecular Excited-State Charge-Transfer Dynamics and Small-Chain Relaxation

Y. Wang, M. C. Crawford,† and K. B. Eisenthal*

Contribution from the Department of Chemistry, Columbia University, New York, New York 10027. *Received January 12, 1982*

Abstract: Intramolecular charge transfer has been observed for the molecule anthracene-$(CH_2)_3$-*N*,*N*-dimethylaniline [9-[3-[4-(dimethylamino)phenyl]propyl]anthracene] in nonpolar solvents of varying viscosities. The technique employed was picosecond time-resolved fluorescence utilizing a Nd^{3+}:phosphate glass laser and streak camera. Measurements of the fluorescence decay of the excited-state acceptor (anthracene moiety) and the fluorescence rise of the exciplex demonstrate that there is no intermediate nonfluorescent state existing prior to exciplex formation and that the end-to-end cyclization of the four-bond methylene chain is exponential in time. This exponentiality has not been previously demonstrated. Furthermore, a dependence of exciplex rise time upon the fluorescence wavelength is found and interpreted as evidence for two distinct ground-state conformers, one being dominant. Each conformer has a different viscosity dependence for the formation of an exciplex. General conclusions concerning charge-transfer dynamics in solution are presented on the basis of these and related studies.

Charge-transfer (CT) interactions of excited molecules with neighboring molecules play a vital role in electronic energy relaxation. The quenching of excited-state fluorescence and either the appearance of a new, red-shifted exciplex emission or the formation of ion radicals are manifestations of charge-transfer phenomena. The widespread interest and importance of these light-driven charge generation processes is reflected by the numerous studies[1] on this subject since the discovery of the perylene–dimethylaniline exciplex by Leonhardt and Weller.[2] Two questions concerning the nature of the excited CT interaction are particularly interesting, namely the dependence of reaction on distance and geometry. From studies of *intermolecular* exciplex formation between anthracene and diethylaniline molecules using picosecond transient absorption,[3] it has been concluded that when the two molecules are separated by $\simeq 8$ Å, rapid exciplex formation (10^{11} M^{-1} s^{-1}) occurs. For study of the geometric requirements for exciplex formation, one approach is to restrict the relative orientation of the electron donor and acceptor molecules by connecting them with a number of methylene groups.[4-11] The effect of this restriction on the formation of the *intramolecular* exciplex is then studied.

In an earlier communication,[11] we reported preliminary results on the study of the intramolecular exciplex 9-anthracene-$(CH_2)_3$-*p*-*N*,*N*-dimethylaniline

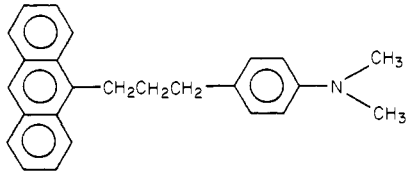

in isopentane solution. On the basis of the dynamics we concluded that internal rotational motions are required to achieve a favorable geometry for the formation of the intramolecular exciplex in the nonpolar solvent. The observation of a dependence of exciplex rise time upon the fluorescence wavelength monitored was interpreted as evidence for two groups of distinct ground-state conformers. We have now extended this study to solvents of widely

Table I. Time Constants for Intramolecular Exciplex Formation in Various Solvents; Uncertainty in Lifetimes Is ±10%

solvent	isopentane	hexane	decane	tetradecane
viscosity, cp	0.22	0.33	0.92	2.18
dielectric constant	1.84	1.89	1.99	
anthracene moiety decay at 410 nm, ns	1.4	1.9	2.8	3.8
CT formation at 480 and 520 nm, ns	1.4	1.9	2.9	4.1
CT formation at 570 and 600 nm, ns	2.0	2.6	3.8	5.5

† IBM predoctoral fellow.

(1) (a) H. Beens and A. Weller in "Organic Molecular Photophysics", T. B. Birks, Ed., Wiley, New York, 1975, Vol. II. (b) N. Mataga and M. Ottolenghi in "Molecular Association", R. Forster, Ed., Academic Press, New York, 1979, Vol. II.
(2) H. Leonhardt and A. Weller, *Ber. Bunsenges. Phys. Chem.*, **67**, 791 (1963).
(3) T. J. Chuang and K. B. Eisenthal, *J. Chem. Phys.*, **59**, 2140 (1973); **62**, 2213 (1975).
(4) E. A. Chandross and H. T. Thomas, *Chem. Phys. Lett.*, **9**, 393 (1971).
(5) T. J. Chuang, R. J. Cox, and K. B. Eisenthal, *J. Am. Chem. Soc.*, **96**, 6828 (1974).
(6) R. S. Davidson and V. R. Tretheway, *J. Chem. Soc., Chem. Commun.*, 827 (1976).
(7) R. Ide, Y. Sakata, and S. Misumi, *J. Chem. Soc., Chem. Commun.*, 1009 (1972).
(8) T. Okada, T. Fujita, M. Kubota, S. Masaki, N. Mataga, R. Ide, Y. Sakata, and S. Misumi, *Chem. Phys. Lett.*, **14**, 563 (1972).
(9) J. H. Borkent, A. W. J. De. Jong, J. W. Verhoeven, and Th. J. De Boer, *Chem. Phys. Lett.*, 57, 530 (1978).
(10) F. Pragst, H. J. Hamann, K. Teuchner, and S. Daehne, *J. Lumin.* **17**, 425 (1978).
(11) Y. Wang, M. K. Crawford, and K. B. Eisenthal, *J. Phys. Chem.*, **84**, 2696 (1980).

0002-7863/82/1504-5874$01.25/0